PHYSICS OF FLUIDS **27**, 036601 (2015)

Gravity currents propagating up a slope in a two-layer fluid

Larissa J. Marleau,[1,a)] Morris R. Flynn,[1,b)] and Bruce R. Sutherland[2,c)]
[1]*Department of Mechanical Engineering, University of Alberta, Edmonton, Alberta T6G 2E1, Canada*
[2]*Departments of Physics and of Earth and Atmospheric Sciences, University of Alberta, Edmonton, Alberta T6G 2E3, Canada*

(Received 5 November 2014; accepted 27 February 2015; published online 16 March 2015)

Gravity currents produced by partial-depth lock-release and travelling along the base of a two-layer stratified ambient are investigated as they propagate along a rising slope. The initial gravity current front speed is found to be consistent with a theory adapted from Shin *et al*. ["Gravity currents produced by lock exchange," J. Fluid Mech. **521**, 1-34 (2004)] to the case of partial-depth currents in two-layer ambients. The subsequent evolution depends on the gravity current speed relative to the speed of the interfacial disturbance it creates. The deceleration of supercritical gravity currents, which travel faster than the interfacial disturbance, is gradual and agrees well with the relationship developed by Marleau *et al*. ["Gravity currents propagating up a slope," Phys. Fluids **26**, 046605 (2014)] for upslope gravity currents in uniform density ambients. In several subcritical cases, the gravity current suddenly came to rest as a consequence of interactions with the interfacial disturbance. The disturbance amplitude, speed, and width are found to be nearly constant during its evolution. In cases for which the ambient interface intersected the bottom slope, the amplitude, speed, and width were nearly constant up to the point where the lower layer shallowed and the disturbance transformed into an upslope-propagating gravity current. © *2015 AIP Publishing LLC.* [http://dx.doi.org/10.1063/1.4914471]

I. INTRODUCTION

A gravity current is a primarily horizontal flow caused by density differences between the current fluid and the ambient fluid.[1–3] Some examples of gravity currents found in nature are cold-air outflows from thunderstorms, dust storms (haboobs), turbidity currents running down the continental shelf, and advancing cold fronts. Examples of gravity currents found in industrial processes are the spread of heavy gases and also ventilation systems that utilize buoyancy to drive horizontal flows along the ceiling and floor.[2] Many studies have investigated gravity currents by way of theory, laboratory experiments, and numerical simulations. Most of these focused upon the special case in which the gravity current travelled along a horizontal surface[4–12] or over small obstacles.[13,14]

To predict the speed of a gravity current, Benjamin[6] used a reference frame fixed to the gravity current front and required mass and momentum conservation. This model allowed him to derive a formula for the front speed with respect to the heights of the gravity current and ambient and the density difference between the two fluids. By additionally assuming energy conservation, he showed that the gravity current head should occupy half the ambient depth. The prediction was confirmed by the results of full-depth lock-release experiments. Through experiments with a finite volume of lock-fluid and using a theory that combined Benjamin's front condition with shallow water theory, Rottman and Simpson[10] showed that a gravity current that originates from

a)Email: lmarleau@ualberta.ca
b)Author to whom correspondence should be addressed. Electronic mail: mrflynn@ualberta.ca. URL: websrv.mece.ualberta.ca/mrflynn.
c)Email: bruce.sutherland@ualberta.ca. URL: www.ualberta.ca/~bsuther.

a full-depth lock propagates six to ten lock-lengths at constant speed. The flow then transitions to a buoyancy-inertia self-similar phase during which the front speed decreases with respect to time.[9,10,15] Several investigations of gravity currents arising from partial-depth lock-release experiments have also been conducted. Among these, Shin *et al.*[11] adapted Benjamin's theory assuming that the return flow into the lock takes the form of an internal bore. Thus, they developed an equation for the speed of energy conserving gravity currents and found their prediction to be consistent with experimental measurements. All of these investigations were for the case of horizontally propagating gravity currents in a uniform ambient.

Several studies have considered horizontally propagating gravity currents in a two-layer ambient fluid.[16–20] Rottman and Simpson[21] compared a gravity current moving over a horizontal bottom beneath a two-layer ambient to a symmetric, streamlined obstacle being towed beneath a two-layer ambient, as was studied by Baines.[14] Comparing their theory to laboratory experiments, Rottman and Simpson found that interfacial disturbances created by gravity currents took on forms ranging from long waves to undular and turbulent bores depending on the ambient conditions and initial conditions of the lock-release experiments. In experiments of intrusive gravity currents in two-layer, three-layer, and uniformly stratified fluids, the flow was observed to excite internal solitary waves that then acted upon the currents causing them to halt abruptly or, in symmetric circumstances, propagate long distances at constant speed.[18,22,23]

Regarding downslope flow, saline gravity currents were found to propagate at constant speed far downslope in a fresh water ambient due to a balance between the accelerating effect of gravity and the decelerating effects of bed friction and ambient entrainment.[24–27] In contrast, upslope-propagating gravity currents in uniform ambients decelerate.[28,29] In their investigation of full- and partial-depth lock-release gravity currents on slopes ranging from 0.25 (14°) to 1.13 (48°), Marleau *et al.*[28] developed a theory for the frontal deceleration, which agreed well with experimental results.

The investigation reported upon here extends the work of Marleau *et al.*[28] by considering the effects of stratification upon the evolution of upslope propagating gravity currents released from a partial-depth lock in a two-layer fluid. As well as providing a better understanding of such a fundamental phenomenon, the work provides insight into the evolution of sea breezes as they advance inland and uphill from the coast in the presence of an atmospheric inversion. Such sea breezes are known to provide a crucial supply of moisture to inland crops, as in the case of the wineries on a plateau northeast of Santa Barbara, California.

In Sec. II, existing predictions for the gravity current speed, upslope deceleration, and stopping distance are extended to the case of a two-layer ambient. Predictions for the amplitude of interfacial disturbances excited by the advancing current are also reviewed. Section III describes the set-up of the lock-release experiments and the analysis techniques used in processing experimental images. Also described are qualitative observations of the formation and evolution of the gravity current and interface displacement. In Sec. IV, measurements of the gravity current front speed are compared against both theoretical predictions and the speed of the interfacial disturbance. Measurements of the gravity current deceleration and stopping distance are presented along with measurements of the interfacial disturbance amplitude, width, and speed. Wherever possible, these are compared against theory. Finally, Sec. V gives a summary of key results.

II. THEORY

A. Initial gravity current speed

The prediction for the front speed, U_{GC}, of an inviscid, steady-state gravity current was first presented by Benjamin[6] who considered a gravity current propagating through a uniform ambient fluid of depth H. Benjamin described the front speed in terms of a Froude number, Fr,

$$U_{GC} = \mathrm{Fr}\sqrt{g'H}, \tag{1}$$

in which $g' = g(\rho_0 - \rho_2)/\rho_{00}$ is the reduced gravity based on the density, ρ_0, of the gravity current and the density, ρ_2, of the ambient fluid. In the Boussinesq approximation, ρ_{00} is a reference density taken to be any value between ρ_2 and ρ_0. Benjamin predicted $\mathrm{Fr} = [\delta(1-\delta)(2-\delta)/(1+\delta)]^{1/2}$, where

$\delta \equiv d/H$ is the ratio of the gravity current height, d, to the ambient depth, H. Additionally, assuming energy conservation, he found that $\delta = d/H = 1/2$, for which Fr = 1/2.

For partial-depth lock-release experiments, in which the dense lock-fluid, initially behind the gate, does not span the entire channel depth, Shin *et al.*[11] considered the advance of the dense fluid, together with the return flow of ambient fluid into the lock to predict the front speed of energy conserving gravity currents. They predicted the height of the steadily advancing gravity current to be half the initial height, D, of the dense lock-fluid and found the speed to be given by (1), in which the Froude number is

$$\mathrm{Fr} = \sqrt{\delta(1-\delta)}, \tag{2}$$

with $\delta = D/2H$. The equation above reproduces Benjamin's energy conserving result in the limit $D \to H$.

Here, the Shin *et al.*[11] result is extended to predict the front speed for a partial-depth lock-release flow in a two-layer stratified ambient. The upper-layer depth and density are $H - h$ and ρ_2, respectively, and the lower-layer depth and density are h and ρ_1, respectively. We suppose that a gravity current results from the release of lock-fluid having density ρ_0 ($> \rho_1 > \rho_2$) and depth D ($> h$) above the bottom. The depth-weighted mean density of the ambient fluid outside the lock from the bottom to height D is $\overline{\rho} = (1 - h/D)\rho_2 + (h/D)\rho_1$. It is assumed that the initial front speed is set by the density difference between the lock-fluid and $\overline{\rho}$, as expressed through the reduced gravity by $\overline{g}' = g(\rho_0 - \overline{\rho})/\rho_{00}$. Thus, using (1) and (2), the speed is predicted to be

$$U_{GC} = \frac{1}{2}\sqrt{(D - hS)(2 - D/H)g'_{02}}, \tag{3}$$

where $S = (\rho_1 - \rho_2)/(\rho_0 - \rho_2)$ is the stratification parameter introduced by Ungarish,[15] and $g'_{02} = g(\rho_0 - \rho_2)/\rho_2$ is the reduced gravity based on the lock-fluid and upper-layer ambient density. This prediction will be compared with experimental results.

B. Gravity current deceleration and stopping distance

Although the above result is derived in the limit of negligibly small slope, s, it should remain applicable in the case of small s at early times (some symbols appear in Figure 1 for reference). For longer times, the front speed is expected to vary with time at least in part as a consequence of running upslope against gravity, but also as a consequence of the changing relative depths of the upper and lower layer fluids. The along-slope deceleration, d_x, of upslope flow in a uniform ambient was considered by Marleau *et al.*[28] who assumed that the Froude number, Fr, of a full- or partial-depth lock-release gravity current is constant even as the ambient depth decreases. Their prediction for d_x, which is constant for flow up a uniform slope, was shown to be in good agreement with laboratory measurements (e.g., see Figure 2(e) of Marleau *et al.*[28]). This result is readily adapted here by replacing the reduced gravity in their equation with $\overline{g}'$ as above Eq. (3), but now accounting for the fact that the lower-layer depth is a decreasing function of the along-slope coordinate, x. Explicitly, the mean density ahead of the dense fluid is

$$\overline{\rho}(x) = \left(1 - \frac{h - sx}{D}\right)\rho_2 + \frac{h - sx}{D}\rho_1, \tag{4}$$

in which the bottom has uniform slope, s, and $x = 0$ corresponds to the position where the gravity current speed, U_{GC}, is given by (3). Hence, the front speed as a function of x is written as

$$\frac{\mathrm{d}x}{\mathrm{d}t} = \mathrm{Fr}\left[\overline{g}'(x)H_s(x)\right]^{1/2}, \tag{5}$$

in which Fr is given by (2), $\overline{g}'(x) = g(\rho_0 - \overline{\rho}(x))/\rho_{00}$, and $H_s(x) = H - sx$ is the total ambient depth. This differential equation can be integrated to obtain an expression for the front position, x_f, in terms of time,

$$x_f(t) = \frac{H}{2s\kappa}\left[\kappa - 1 + (\kappa + 1)\sin\left(\frac{s}{2H}\sqrt{S(2H - D)g'_{02}}\,t + C\right)\right], \tag{6}$$

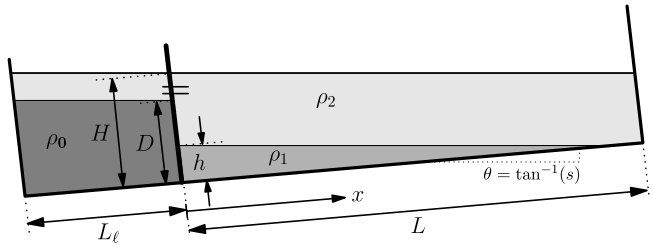

FIG. 1. Schematic side-view of the laboratory set-up before the start of an experiment with salt water of density ρ_0 and lock-gate depth D (dark grey) located behind a gate in a lock of length L_ℓ. The lower layer ambient fluid is salt water with density ρ_1 and lock-gate depth h (medium grey). The upper ambient fluid is fresh water with density ρ_2 and depth $H-h$ (light grey). The tank is angled such that the bottom surface has slope s, which is here exaggerated for clarity. The gate is oriented normal to the tank bottom.

in which $\kappa \equiv HS/(D - hS)$. The constant C is determined from the initial condition $x(0) = 0$, which gives

$$C = \sin^{-1}\left(\frac{1-\kappa}{1+\kappa}\right).$$

Unlike upslope motion in a uniform density ambient,[28] here the deceleration is not uniform. The maximum deceleration, determined from (6), is

$$d_x = \frac{1}{8}g'_{02}s\left(\frac{D}{H} + S(1 - h/H)\right)\left(2 - \frac{D}{H}\right). \tag{7}$$

Finally, the maximum upslope distance is found to be

$$x_{\max} = \frac{H}{s}. \tag{8}$$

This result is unphysical in the case of small D because according to (4), Eq. (6) is valid only for $x_f < h/s$. Under the assumption that the deceleration is constant and equal to (7), a more broadly applicable estimate for $x_{\max}$ is

$$x_{\max} = \frac{H}{s}\left(\frac{1}{1+\kappa}\right). \tag{9}$$

The influence of interfacial disturbances generated by the gravity current in a two-layer ambient is neglected in deriving (6) and (9). As will be argued in Sec. IV, these disturbances can exert a substantial dynamical impact if the initial current speed is much slower than the disturbance speed.

C. Interfacial disturbance properties

Tan *et al.*[19] predicted the amplitude, A, of the ambient interfacial disturbance caused by a partial-depth lock-release gravity current propagating along a horizontal bottom through a two-layer stratified ambient with upper-layer depth $H - h$ and lower-layer depth h. By first applying Bernoulli's equation in the upper and lower ambient layers for the full-depth case ($D = H$), they found that $A = (H - h)/2$. In that circumstance, it is known that the current depth is half the ambient depth: $d = H/2$. Thus, the amplitude of the interfacial disturbance resulting from a full-depth lock-release can be written as

$$A = d\left(1 - \frac{h}{H}\right). \tag{10}$$

Assuming d/D decreases linearly as D/H increases, consistent with the experimental data of Rottman and Simpson,[10] and requiring $d = H/2$ when $D = H$, the current depth as a function of lock-depth is estimated to be

$$d = D\left[\alpha - (\alpha - \tfrac{1}{2})\frac{D}{H}\right], \tag{11}$$

where $\alpha \simeq 0.87$ is a fitting parameter determined from Figure 10 of Rottman and Simpson.[10] Combining (11) with the limiting case of (10) gives a prediction for the relative interfacial disturbance amplitude, nondimensionalized by the harmonic mean of the ambient layer depths, $\overline{H} = h(H-h)/H$,

$$\frac{A}{\overline{H}} = \frac{D}{h}\left[\alpha - (\alpha - \tfrac{1}{2})\frac{D}{H}\right]. \tag{12}$$

III. EXPERIMENT SET-UP AND ANALYSIS

A. Tank set-up

The experimental set-up is illustrated schematically in Figure 1. All experiments were performed in a long, rectangular, glass tank of interior length $L + L_\ell = 197.5$ cm, width 17.6 cm, and total height 48.5 cm. In some experiments, the tank was laid flat. But in most instances, one end of the tank was raised so that the bottom slope was $s = 0.026$ (1.5°), $s = 0.052$ (3.0°), or $s = 0.079$ (4.5°).

First, the tank was filled with dyed salt water of density ρ_1 to a height $h = 10.0$ cm, as measured at a distance $L_\ell = 40.0$ cm from the lock-end of the tank. A watertight gate was then inserted at this position, and fresh water having density, ρ_2, was slowly added to the ambient region through a sponge float, which was used to decrease mixing at the interface between the fresh and salt water layers. The resulting interface thickness was typically 0.5 cm, sufficiently thin to approximate the ambient as a two-layer fluid. Simultaneously, fresh water was slowly poured into the lock so that the total fluid depths on either side of the gate were approximately equal. The addition of fluid continued until the free surface inside and outside of the lock was just below a series of sponge-covered perforations that were located 20 cm above the bottom of the gate. Salt and dye were then mixed into the lock so that the resulting lock-fluid density was $\rho_0 > \rho_1$. Thereafter, more fresh water was added to the ambient fluid so that the ambient free surface rose above the level of the perforations, flowed into the lock through the perforations and overlaid the dense lock-fluid. Concurrently, dense fluid was slowly siphoned out of the lock at the same rate as fluid was added, until the dense layer had the prescribed depth, D. Once the filling process was complete, the siphon and sponge float were removed. At this point, the lock and ambient fluid each had a total height H at the position of the lock-gate.

All experiments involved a partial-depth lock-release. The lock-depth, D, ranged from 10 cm to 20 cm, and H was fixed at 30.0 cm in all experiments so that the ratio of lower-layer to total ambient depth was always close to 1/3. Because the slope angle $\theta = \tan^{-1}(s) \leq 4.5°$ in all cases, the fluid depths measured perpendicular to the sloped bottom were approximately equal to the corresponding vertical depths. For example, although H was measured as the distance from the bottom of the gate to where the free surface meets the gate (see Figure 1), its value is taken to represent the approximate vertical distance from the bottom of the gate to the surface.

The lock density, ρ_0, ranged from 1.0020 g/cm^3 to 1.0200 g/cm^3. The lower-layer ambient density, ρ_1, ranged from 1.0005 g/cm^3 to 1.0100 g/cm^3, in all cases being less than the lock density. Finally, the upper layer had an average density of 0.9986 g/cm^3. Fluid densities were, in all cases, measured using an Anton Paar DMA 4500 density meter, which had a precision of ±0.000 01 g/cm^3.

The Reynolds number based on the lock-depth and density difference between the lock-fluid and the lower layer ambient was given by $\mathrm{Re} = D\sqrt{g'_{02}D}/\nu$ in which $\nu = 0.01$ cm^2/s is the kinematic viscosity. In our experiments, Re ranged between $\mathrm{Re} = 6 \times 10^3$ and 7.5×10^4, sufficiently large that viscous dissipation was not expected to play a dominant role.

For all of the experiments, a bank of fluorescent bulbs was placed behind the tank. Two translucent white plastic sheets were located between the lights and the tank to provide nearly uniform background illumination. Movies of the experiments were recorded using a Canon EOS Rebel T3i digital camera. This was situated approximately 3 m in front of the tank, midway along its length, and midway between the free surface and bottom of the tank. The field-of-view was set so that the entire tank length, including the lock region, was included.

B. Observations and analyses

Each experiment began by swiftly extracting the gate. The dense lock-fluid then collapsed beneath the lower-layer ambient as a gravity current. Typically, the collapse also generated a large hump-shaped interfacial disturbance ahead and above the developing gravity current. The disturbance resembled a solitary wave except that dense lock-fluid appeared, at least at early times, beneath the crest of the disturbance. As the gravity current propagated upslope, a progressively greater volume of dense fluid drained back toward the lock. In part, this was due to gravity. But in many experiments, the draining was also influenced by a transfer of momentum between the current and the interfacial disturbance.

In order to measure the evolving structures of both the gravity current and the interfacial disturbance, along-slope time-series plots of gravity current height and interface displacement were constructed for each experiment. The construction was performed using Matlab, which located in each video frame the interface between the two ambient layers and the interface between the current and lower-layer ambient. From these images, the height of the gravity current above the tank bottom and the interface displacement were computed as functions of the along-slope distance, x, from the lock-gate. In practice, these heights were computed for x in the range $0.5L_\ell < x < L - 0.5L_\ell$. This interval was chosen deliberately to exclude the initial collapse of the gravity current and the initial formation of the interfacial disturbance. It also excluded the interaction of the interfacial disturbance and/or the gravity current with the right end-wall of the tank. The above process was repeated at successive times to produce time-series of gravity current height and interface displacement as functions of along-slope distance and time. From the slope of contours in these plots, the speeds of the gravity current and interfacial disturbance, U_{GC} and U_{ID}, were computed. Details of how these speeds were measured are given at the end of this section.

The experiments showed different qualitative behaviours depending upon the speed of the gravity current relative to the interfacial disturbance. In an effort to be objective in grouping together gravity currents having similar qualitative properties, the currents were classified as subcritical, critical, or supercritical depending on their speed relative to the interfacial disturbance speed. Explicitly, gravity currents were called supercritical if $U_{GC} > 1.04\,U_{ID}$, subcritical if $U_{GC} < 0.96\,U_{ID}$, and critical otherwise.

For example, Figure 2 shows the results of a supercritical gravity current experiment. Figure 2(a) presents a snapshot of the experiment taken 20 s after the gate was extracted (at $t = 0$). Here, the dark-dyed current is seen to underlie the interfacial disturbance between the clear fresh layer and light-dyed lower ambient layer. Figure 2(b) plots the gravity current height, $d(x,t)$, nondimensionalized by the lock-depth, D. As expected, the maximum height was approximately $D/2$ shortly after release. At early times, the gravity current front maintained a nearly constant speed as it propagated upslope. This is evident from the near-constant slope of the $d \simeq 0.3D$ contour in Figure 2(b). While running up the slope, the gravity current head decreased in height and length as dark-dyed fluid continually drained downslope. Figure 2(c) shows the displacement of the interface nondimensionalized by D. This panel indicates that, shortly after generation, the interfacial disturbance travelled with a near-constant speed, amplitude, and width even as the gravity current advanced to the leading edge of the disturbance, at which point the gravity current depth and interface displacement became equal.

To better illustrate the interaction between the current and interface, close-up snapshots of this experiment at late times are shown in Figure 3. These show that the turbulence behind the head of the gravity current is partially suppressed as the thickness of the lower-layer ambient about the head decreases. After the gravity current penetrates through the lower layer, the head is surrounded by a uniform ambient of density, ρ_2, and larger turbulent fluctuations about the head are again observed. This same phenomenon was seen in all supercritical cases in which the two-layer ambient interface intersected the slope and the gravity current front penetrated into the upper layer. The observations suggest that the close proximity of a density interface can partially suppress mixing and entrainment into the current head.

Figure 4 shows an example of a critical experiment, for which the current and disturbance speed are roughly equal. In the snapshot of Figure 4(a), the gravity current head is surrounded by lower-layer fluid far along its length, as compared to the supercritical current shown in Figure 2(a). The time-series

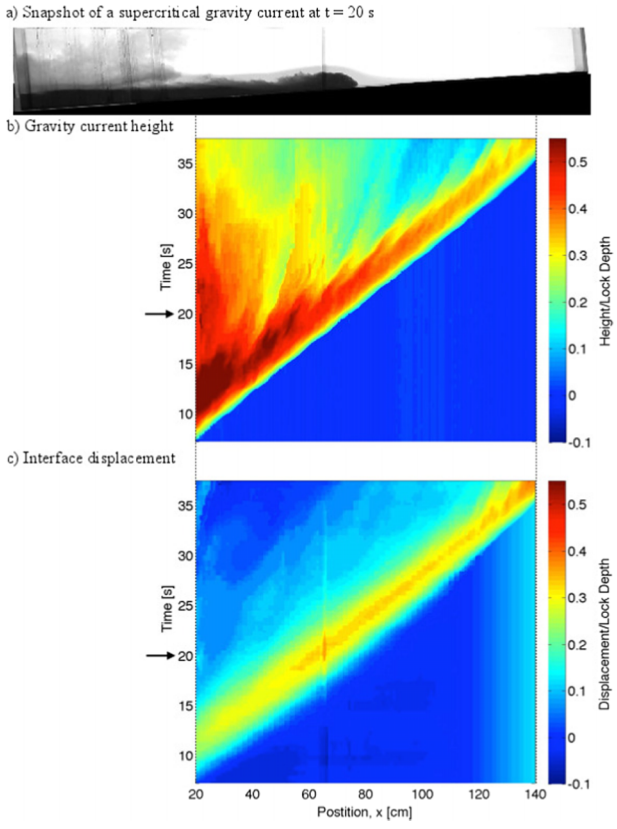

FIG. 2. Supercritical experiment snapshot with the field-of-view showing the entire tank (a), gravity current height (b), and interface displacement (c). The arrows at $t = 20$ s in panels (b) and (c) indicate the time of the snapshot in panel (a). The experimental parameters were $D/H = 0.47$, $s = 0.079$ ($\theta = 4.5°$), $\rho_0 = 1.0064$ g/cm^3, $\rho_1 = 1.0014$ g/cm^3, and $S = 0.36$. The apparent vertical line at $x \simeq 65$ cm is the result of the seam between the two plastic sheets behind the tank.

of the gravity current height in Figure 4(b) exhibits similar features to those of the supercritical current. In particular, the front advances at near-constant speed. Behind the head, however, dense fluid in the tail decelerates through a series of distinct pulses. In other experiments of critical gravity currents, a slight deceleration of the front and/or the formation of a secondary front was observed (features commonly observed for subcritical currents, as discussed in more detail below). Like the supercritical case, the interfacial disturbance, shown in Figure 4(c), is seen to maintain a near-constant speed,

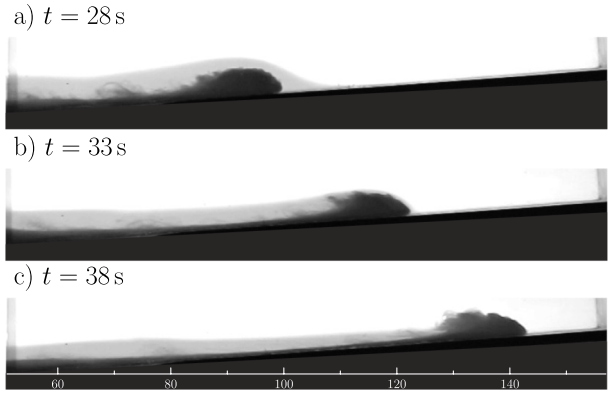

FIG. 3. Close-up snapshots of the supercritical gravity current shown in Figure 2 at times (a) $t = 28$ s, (b) 33 s, and (c) 38 s. The field-of-view shows a portion of the tank far from the lock; the scale below panel (c) indicates the horizontal position from the lock-gate with distances measured in cm.

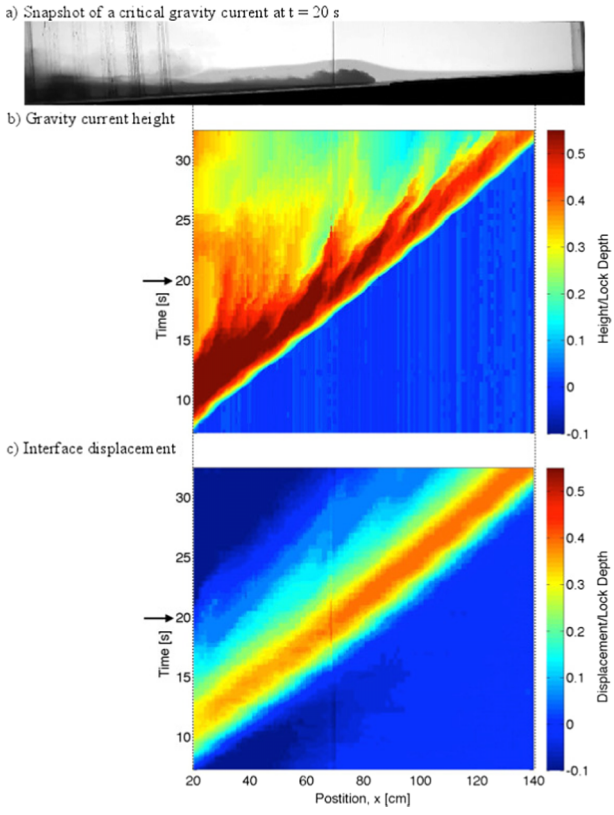

FIG. 4. As in Figure 2 but showing an example of a critical flow with $D/H = 0.33$, $s = 0.052$ ($\theta = 3°$), $\rho_0 = 1.0083$ g/cm^3, $\rho_1 = 1.0017$ g/cm^3, and $S = 0.34$.

amplitude, and width. In this case, however, the gravity current does not overtake the interfacial disturbance.

Figure 5 shows the results from a subcritical gravity current experiment, for which the gravity current speed was less than the interfacial disturbance speed. In the snapshot taken 20 s after release, shown in Figure 5(a), the gravity current has a thin front at $x \simeq 80$ cm and a trailing bulge at $x \simeq 50$ cm. These features differ qualitatively from those of supercritical gravity currents which exhibit the more familiar raised head with turbulent structures in the lee. The evolution of the thin front and trailing bulge can be tracked in Figure 5(b). The gravity current head had a maximum nondimensional height of 0.40, at $x = 20$ cm, $t = 10$ s after release from the lock. Thereafter, it propagated at near-constant speed, but the head height decreased rapidly until the front abruptly halted. After the front came to rest, the fluid inside the head continued to drain downslope, thus preventing the front from continuing its upslope propagation. While the primary head propagated upslope, a second head developed behind it with a maximum nondimensional height of $d/D \simeq 0.45$ at $t = 16$ s. This secondary head also propagated rightward at near-constant but slower speed while the head height rapidly decreased until the secondary front halted. Figure 5(c) shows that the interfacial displacement likewise formed a disturbance that surrounded the primary gravity current head but which continued to propagate at constant speed even after the primary front stopped. A trailing interfacial disturbance also developed surrounding the secondary gravity current head. This too travelled at near-constant speed to the end of the tank after the secondary front halted. The secondary gravity current head and secondary interfacial disturbance were present in most subcritical gravity current experiments and even some of the critical experiments. The observed sudden halting of the current front and the steady advance of the interfacial disturbance was typical of subcritical gravity current experiments. These observations are consistent with observations of experiments of horizontally propagating gravity currents and intrusions in stratified fluid.[10,18,22,23,30] Hence, the bottom slope in our experiments was not expected to

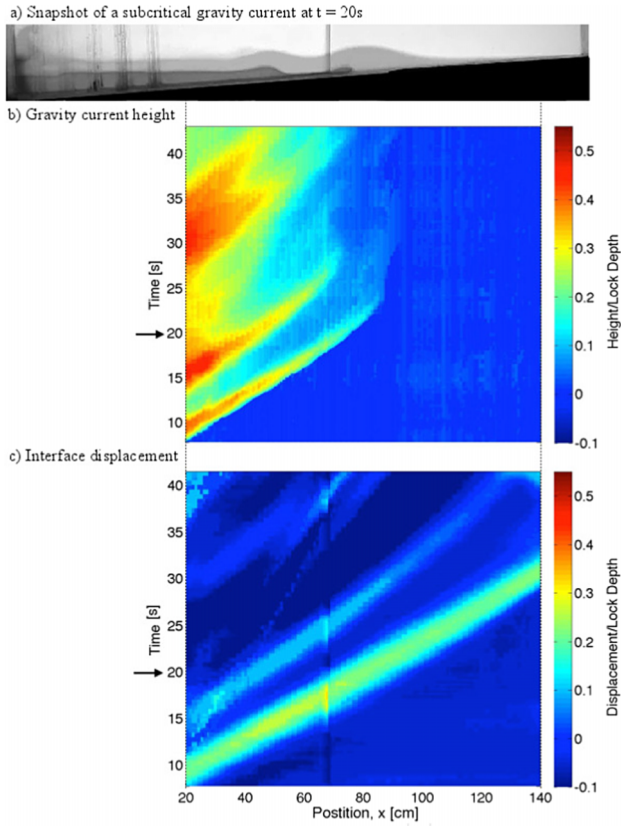

FIG. 5. As in figure 2 but showing an example of a subcritical flow with $D/H = 0.33$, $s = 0.052$ ($\theta = 3°$), $\rho_0 = 1.014$ g/cm^3, $\rho_1 = 1.008$ g/cm^3, and $S = 0.62$.

play a significant qualitative role in the formation of primary and secondary fronts and their sudden stopping during subcritical experiments.

However, the slope did play a role in the consequent evolution of the interfacial disturbance which, after leaving the gravity current behind, continued to propagate rightward as a shoaling internal solitary wave. As the lower layer shallowed to zero depth, the wave then transformed into a gravity current all the while maintaining its speed, as shown in Figure 6. Of course at longer times if not colliding with the end-wall of the tank, this newly developed gravity current would gradually decelerate and stop, as predicted by Marleau *et al.*[28]

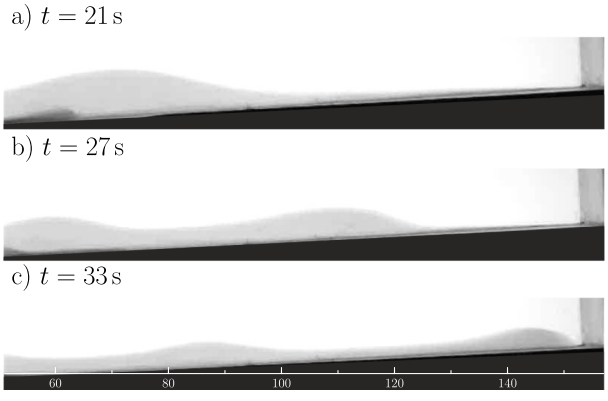

FIG. 6. Close-up snapshots of the subcritical gravity current experiment shown in Figure 5 focusing on the shoaling interfacial disturbance at times (a) $t = 21$ s, (b) $t = 27$ s, and (c) $t = 33$ s. The field-of-view shows a portion of the tank far from the lock; the scale below panel c indicates the horizontal position from the lock-gate with distances measured in cm.

To measure front speed and deceleration, we first located the front position versus time from along-slope time series of intensity. This position was determined by finding at each along-slope location the time at which the intensity changed most rapidly from relatively bright to dark.

Whether the gravity current was classified as supercritical, critical, or subcritical, the initial front speed, U_{GC}, was found from the slope of the best-fit line through data of the front position *vs* time over the range $0.5L_\ell < x < 1.5L_\ell$. This speed was measured in the x-direction, which is at an angle, $\theta = \tan^{-1}s$, to the undisturbed ambient interface. The x-range was chosen to be the distance over which the current was well formed but not yet significantly influenced by the slope or interfacial disturbance. The initial front speed was found to vary by much less than the representative measurement error (±3%) and so could be approximated as constant at least as far as one lock-length away from the gate.

The deceleration of the gravity current, d_x, was set to be twice the coefficient of the t^2 term found from the best-fit quadratic that was fit to the front position *vs* time data. In most experiments, the range of points used to compute d_x was $L_\ell < x < L - L_\ell$. However, in cases where the front was observed to come to an abrupt halt (e.g., as in the subcritical case shown in Figure 5), d_x was determined up to the position where the front first stopped.

The amplitude, A, of the interfacial disturbance was found by averaging the maximum displacement of the interface over the range $0.5L_\ell < x < L - 0.5L_\ell$. Beyond an initial transient stage, the interfacial disturbance was observed to have an amplitude that was constant within measurement error (±1 cm) as it propagated to the right end of the tank. The amplitude remained constant even in subcritical cases for which the gravity current front halted and the interfacial disturbance, now identified as a solitary wave, shoaled on the bottom slope and transformed itself into a gravity current. Of course, after shoaling occurred, the measurement of wave amplitude, A, became interpreted as a measurement of gravity current head height. The half-width, W, of the interfacial disturbance was found by measuring the distance between positions where the interfacial disturbance had half the maximum height. Measurements of W were made during the time that both positions, one to the left and the other to the right of the maximum, were within the range $0.5L_\ell < x < L - 0.5L_\ell$. The speed, U_{ID}, of the interfacial disturbance was determined by tracking the position of the half-amplitude displacement ahead of the crest. This was found to be a good approximation of the speed of the entire interfacial disturbance, which was observed to undergo little dispersion (e.g., see Figures 2(c), 4(c), and 5(c)).

IV. RESULTS

A. Initial gravity current speed and structure

The gravity current front was found to propagate at a nearly constant speed at early times after the initial collapse of the dense lock-fluid; the bottom slope did not have an appreciable affect on the gravity current front speed within the first lock-length. Figure 7(a) shows the measured Froude number compared to the prediction (3). As defined previously, $\overline{H} = (H - h)h/H$ where $H - h$ and h are the ambient layer heights measured at the gate. The best-fit line through the data (not shown) has a slope of 0.452 (±0.008) which is moderately smaller than the predicted slope of 1/2. However, this result is consistent with the prefactor of 0.45 found in similar gravity current experiments.[11,18,28] Figure 7(b) compares the gravity current front speed, U_{GC}, and the interfacial disturbance speed, U_{ID}. The speeds, U_{GC} and U_{ID}, are nondimensionalized using different scaling parameters. In particular, U_{ID} is scaled by the shallow water speed, $\sqrt{g'_{12}\overline{H}}$ in which $g'_{12} = (\rho_1 - \rho_2)/\rho_2$. Therefore, data for subcritical, critical, and supercritical gravity currents are interspersed amongst each other in this plot. Because the dashed line in Figure 7(b) has unit slope, it is clear that the nondimensional gravity current front speed is always less than the nondimensional interfacial disturbance speed. Whether the gravity current actually travelled faster or slower than the interfacial disturbance depended, of course, on whether the flow was supercritical ($U_{GC} > 1.04U_{ID}$) or subcritical ($U_{GC} < 0.96U_{ID}$), respectively.

In a Boussinesq fluid of total depth H, the maximum speed of a solitary wave is[31]

$$C_{\mathrm{sw,max}} = \frac{1}{2}\sqrt{g'_{12}H}. \tag{13}$$

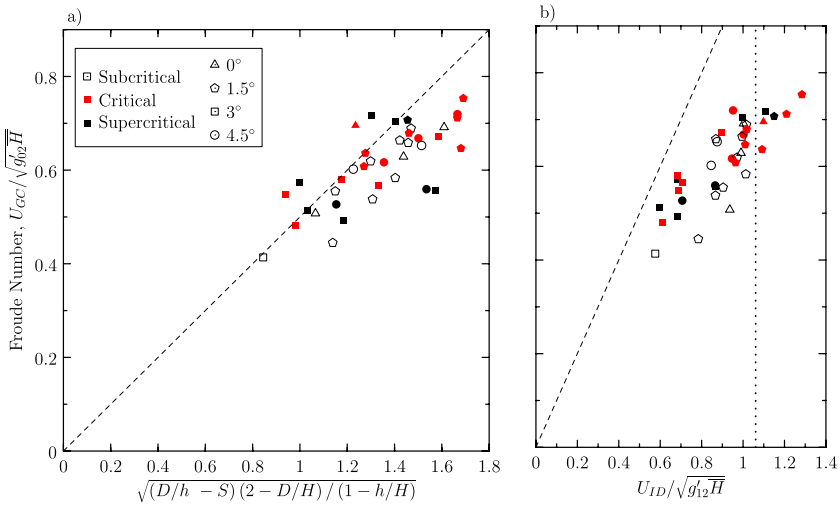

FIG. 7. (a) Measured Froude number *vs* the geometric parameter given by (3). The dashed line has slope 1/2. (b) Measured Froude number *vs* the nondimensionalized interfacial disturbance speed. The dashed line has unit slope. The vertical dotted line indicates the limiting solitary wave speed. Measurement errors are approximately equal to the size of the symbols. In both plots, the shade of symbols represent whether the gravity current is subcritical, critical, or supercritical, and the shape represents the bottom slope, as indicated in the legend of (a).

This maximum speed is realized when the solitary wave amplitude is so large that the crest is at mid-depth, and correspondingly, the speed is that of a shallow water wave in fluid with equal upper- and lower-layer depths. This relative limiting speed in our experiments with $h/H \simeq 1/3$ is indicated by the vertical dotted line at $U_{ID}/\sqrt{g'_{12}\bar{H}} = 3/(2\sqrt{2})$ in Figure 7(b). That in some experiments, the interfacial disturbance had speeds faster than this limit is an indication that the disturbance is not a solitary wave in the usual sense, because it is continually forced by an underlying gravity current. A best-fit line (not shown) through the data has a slope of 0.663 (±0.012), suggesting an approximate empirical relationship,

$$U_{ID} \simeq (1.47 \pm 0.05)\sqrt{S}\, U_{GC}. \tag{14}$$

Baines[14] developed a regime diagram for the qualitative behaviour of a two-layer flow passing over a streamlined obstacle. Rottman and Simpson[21] adapted this analysis by substituting the solid obstacle with a gravity current of non-constant shape propagating over a horizontal boundary beneath a two-layered stratified ambient. Thus, approximating the upper layer as infinitely deep, they determined curves of relative current speed to relative current height that delineated two transitions. One transition occurred between subcritical currents creating symmetric leading and trailing disturbances in the overlying interface and subcritical currents asymmetrically generating interfacial waves that propagate ahead of the current. The other transition occurred between wave-generating subcritical currents and supercritical currents with speeds that exceeded the excited interfacial disturbances. Generally, following Baines,[14] White and Helfrich[32] repeated this analysis for gravity currents in a two-layer fluid of finite depth. They noted that the supercritical boundary occurred for substantially lower relative gravity current speeds if h/H was not negligibly small. Further, they asserted that a better representation of the maximum current speed corresponding to the supercritical boundary was that of the maximum speed of an internal solitary wave, given by (13).

As in Figure 2 of Rottman and Simpson,[21] Figure 8 is a regime diagram in which the relative gravity current speed and height from each experiment are plotted with different symbols depending on the stratification parameter, and whether the measured gravity current speed close to the lock was determined to be subcritical, critical or supercritical with respect to the measured interfacial disturbance speed. Superimposed on each plot are the transition curves predicted from hydraulic theory in the $h/H \to \infty$ limit (dotted line) and in the case of our experiments for which $h/H = 1/3$, using the value of the lower layer depth at the gate (dashed line). Also shown is the supercritical boundary

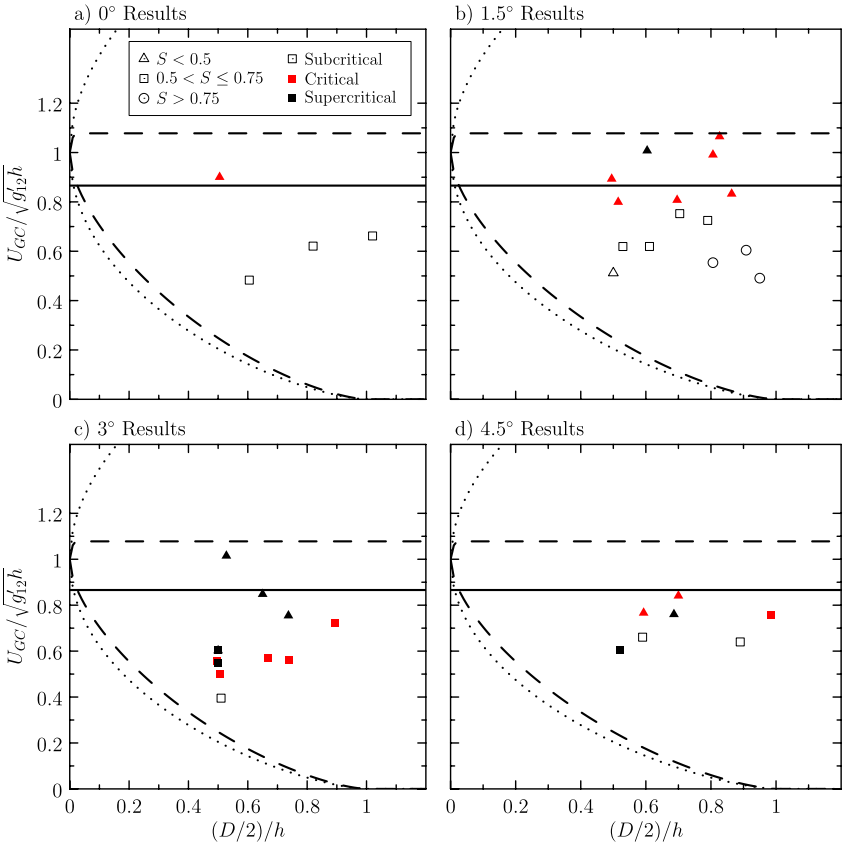

FIG. 8. Nondimensionalized front speed *vs* the geometric parameter $D/2h$. Under the assumption that the current depth d is half the lock-depth ($d = D/2$), the axes are identical to those in Figure 9 of Rottman and Simpson.[21] The transition boundaries from hydraulic theory are plotted for $h/H \to \infty$ (dotted) and $h/H = 1/3$ (dashed). For a given Froude number, $\mathrm{Fr}_h = U_{GC}/\sqrt{g'_{12}h} < 1$, these give the largest possible value of $D/2h$ associated with a symmetric solution of the shallow water equations. For $\mathrm{Fr}_h > 1$, these prescribe the predicted supercritical boundary. The solid line indicates the supercritical boundary determined by the maximum solitary wave speed, $C_{\mathrm{sw,max}}$, relative to $\sqrt{g'_{12}h}$ for the case $h/H = 1/3$. Values of the stratification parameter, S, are represented by the symbol shape. The relative speeds of the gravity current and interfacial disturbance are represented by the symbol shade. These conventions are indicated in the legend in panel (a).

as predicted by the maximum solitary wave speed, $C_{\mathrm{sw,max}}$, computed for the case $h/H = 1/3$ (solid line).

Compared with either prediction of hydraulic theory, all the gravity currents we examined fall within the regime in which the interfacial disturbance above the crest of the gravity current is expected to exhibit upstream and downstream asymmetry associated with upstream wave generation. Consistent with this prediction and with Figures 2(a), 4(a), and 5(a), an asymmetry of the interfacial disturbance was observed in each of our experimental runs. However, it was unclear whether the asymmetry was a due to interactions between the gravity current and interface or instead due to the sloped bottom. For select experiments, the gravity current speed was found to exceed the maximum solitary wave speed, $C_{\mathrm{sw,max}}$. For all these cases, we found the gravity current was indeed critical or supercritical with $S < 0.5$. The points corresponding to subcritical gravity currents all fell below this critical (solid horizontal) line. In other experiments with the slope angles of 3° and 4.5°, the gravity current was found to be supercritical even though its speed was slower than $C_{\mathrm{sw,max}}$. Presumably, this is a consequence of the ambient depth being sufficiently more shallow one lock-length from the gate as to generate an interfacial disturbance with slower maximum speed.

The general trend of increasing stratification parameter S from the top-left to the bottom-right in each panel of Figure 8 is analogous to the trend noted by Rottman and Simpson,[21] who measured

stratification by a parameter, $(\rho_0 - \rho_1)/(\rho_1 - \rho_2)$, which increased from the bottom-right to the top-left of their regime diagram images.

B. Supercritical gravity current deceleration

Over the length of the tank the deceleration, d_x, of supercritical gravity currents was found to be approximately constant even as the current propagated from the lower to the upper layer, as shown in Figures 2 and 3. A similar observation was made by Marleau *et al.*[28] who studied the evolution of an upslope gravity current in a uniform density ambient for a range of upslope angles. In Figure 9 the prediction given by (7) is compared with the measured deceleration determined from the two-layer ambient data and the measured deceleration from Marleau *et al.*[28] When the ambient is uniform $\overline{g}' = g'_{02}$ and $S = 0$, making the axes of Figure 9 equivalent to those in Figure 4 of Marleau *et al.*[28] In the two-layer experiments, the deceleration of supercritical gravity currents with $S < 0.4$ is consistent, within scatter, of the deceleration measured for gravity currents in uniform-density ambients. However, for $S > 0.5$, the measured deceleration is substantially reduced, with no deceleration at all in one case. Thus, even though the gravity current advances initially more quickly than the interfacial disturbance it generated, the disturbance nonetheless has an effect on the consequent evolution of the current if the relative ambient stratification is sufficiently large. Rather than decelerating as a consequence of moving up slope, the current head is carried upslope with the interfacial disturbance at constant speed. The deceleration of critical and subcritical gravity currents (not shown) is poorly predicted by (7) also because of significant interactions with the interface that in some cases carry the current head long distances at constant speed and in others bring the front to an abrupt halt. The uniform advection and the abrupt halting of a gravity current head due to interactions with interfacial disturbances have been noted previously for horizontal gravity currents and intrusions in a two-layer ambient and in uniform stratification.[18,22,23,33]

C. Gravity current stopping distance

In some experiments, whether due to slope or interaction with interfacial disturbances, the deceleration of the gravity current front resulted in it stopping before reaching the end-wall of the tank. Figure 10 shows the measured stopping distance of the gravity current front against the prediction given by (9). Although the prediction assumed that deceleration occurred as a consequence of the decreasing ambient depth with distance from the gate, in reality the gravity currents halted for one of two reasons. In the majority of subcritical cases, the interfacial disturbance extracted momentum as

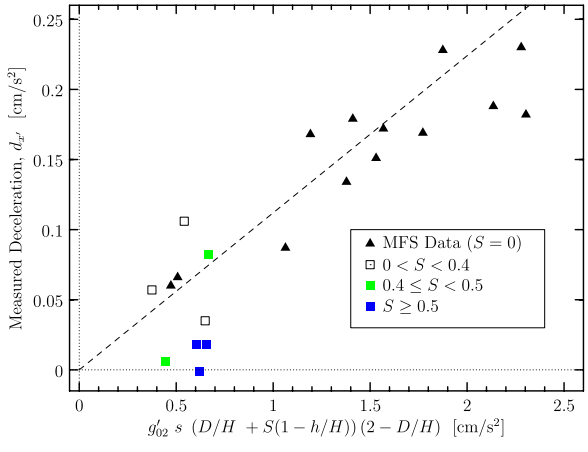

FIG. 9. Front deceleration for the supercritical gravity current experiments with a two-layer ambient (squares) and in uniform density fluid (triangles; from the study of Marleau *et al.*[28]). In the former case, the shade of the square specifies the stratification parameter, S, which ranged between 0.33 and 0.60. The dashed line, with slope 0.112, represents the relationship found in Marleau *et al.*[28] Measurement errors are smaller than the size of the symbols.

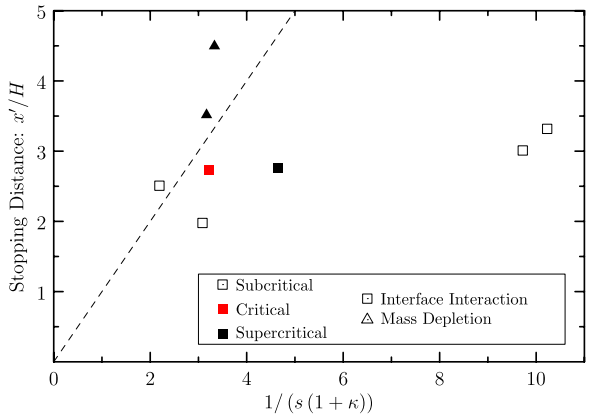

FIG. 10. Measured *vs* predicted stopping distance. The triangles represent experiments in which the gravity current propagation ceased due to fluid flowing back downslope thereby depleting the volume of the head. The squares represent experiments in which the gravity current front decelerated because of an interaction with the interfacial disturbance. Open, red, and black symbols represent subcritical, critical, and supercritical gravity currents, respectively. The dashed line shows the prediction of (9). Measurement errors are approximately half the size of the symbols.

it overtook and arrested the front as the disturbance continued traveling in the downstream direction (e.g., see Figure 5). In other cases, similar to upslope gravity currents in a uniform-density ambient, fluid continually drained downslope from the advancing gravity current until the draining completely depleted the volume of the gravity current head. In most experiments in which gravity currents stopped due to interaction with the interface before reaching the end-wall of the tank, the front halted a distance well before that predicted by (9). Gravity currents that stopped due to mass depletion tended to stop at a distance moderately greater than that predicted by (9).

D. Interfacial disturbance properties

In general, the interfacial disturbance was observed to travel faster for larger A, as shown in Figure 11. This observation is consistent with Korteweg-de Vries (KdV) theory, which predicts that the speed of moderately large solitary waves increases linearly with amplitude. However, the relative amplitudes of the "waves" observed here were comparable to, if not much larger than, the lower ambient depth and were, therefore, much larger than those that can be well-described by KdV theory.[34] Additionally, unlike solitary waves, the interfacial disturbance in most of these experiments had dense gravity current fluid beneath it. In Figure 11, the speed of the interfacial disturbance is nondimensionalized by the shallow water speed, C_0, computed somewhat arbitrarily at $x = L/2$. Specifically,

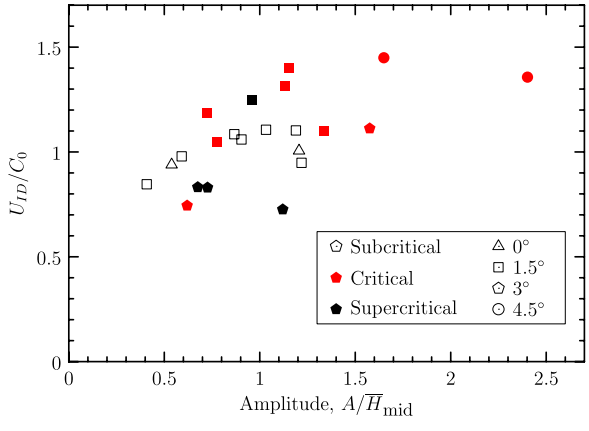

FIG. 11. Interfacial disturbance speed *vs* interfacial disturbance amplitude. Measurement errors are approximately equal to the size of the symbols.

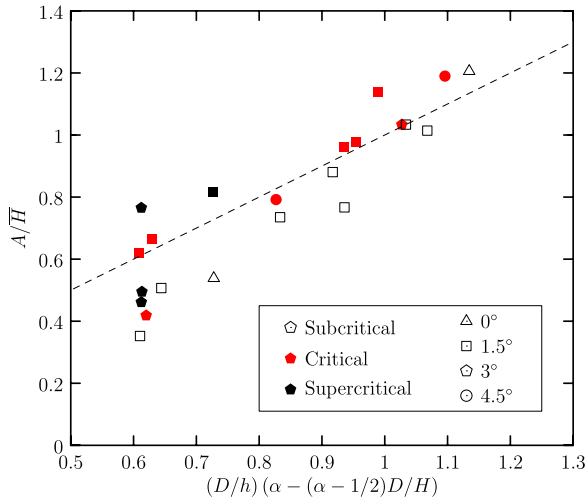

FIG. 12. Scaled interfacial disturbance amplitude *vs* the semi-empirical prediction (12) developed by Tan *et al.*[19] The dashed line uses $\alpha = 0.67$ in (12) rather than $\alpha = 0.87$, the value suggested in this earlier study. Measurement errors are approximately equal to the size of the symbols.

$C_0 = \sqrt{g'_{12}\overline{H}_{\rm mid}}$, in which $\overline{H}_{\rm mid} = (H-h)(h-L\,s/2)/(H-L\,s/2)$. The interfacial disturbance speed exceeded the shallow water speed in the majority of experiments, indicating that the disturbance is a nonlinear phenomenon. The relative speed of disturbances generated by subcritical gravity currents was larger than the relative speed of disturbances generated by supercritical gravity currents.

Figure 12 compares the semi-empirical equation derived from the hydraulic theory of Tan *et al.*[19] against laboratory measurements of the maximum interfacial displacement. Applying the semi-empirical result (12) to our measurements yields $\alpha = 0.67$, somewhat smaller than the Tan *et al.*[19] result of $\alpha \simeq 0.87$.

Figure 13 compares the half-width, W, of the interfacial disturbance to its amplitude, A. Unlike KdV theory, which predicts that W should decrease as A increases, Figure 13 shows that the width increases approximately linearly with amplitude according to $W = (6.9 \pm 0.2)A$. The observation is consistent with the previous experiments examining the properties of solitary waves at amplitudes $A \gtrsim 0.5h$, beyond the realm of KdV theory.[34,35]

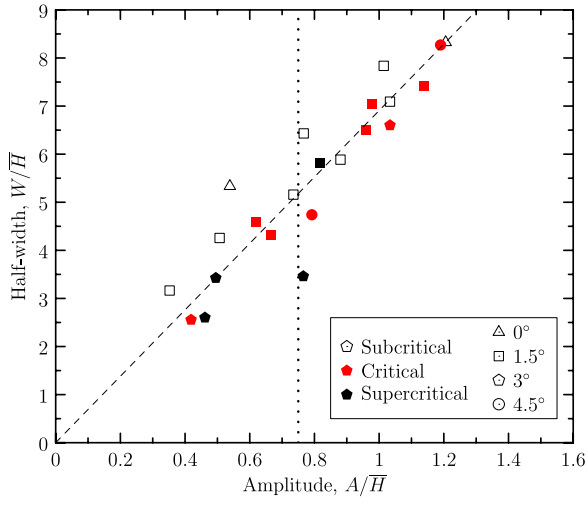

FIG. 13. Scaled half-width of the interfacial disturbance *vs* scaled amplitude of the interfacial disturbance. The dashed line represents the best-fit line. The vertical dotted line indicates the relative amplitude of an interfacial disturbance whose crest lies at mid-depth in the ambient. Measurement errors are approximately equal to the size of the symbols.

But even fully nonlinear solitary waves have limiting amplitudes such that the displaced interface does not exceed the channel mid-depth. The vertical dotted line in Figure 13 shows that this limit is reached in our experiments (with $h/H \simeq 1/3$) when $A/\bar{H} \simeq 3/4$. In many of our experiments, the maximum interface displacement exceeded this value. This is because the interfacial disturbance was not a solitary wave in the usual sense of a nonlinear disturbance in a two-layer fluid. Rather, at least where its properties were measured, the disturbance was continually forced by an underlying advancing gravity current; it was a three-layer disturbance continually forced by a gravity current of progressively diminishing volume.

In presenting data in Figures 11 and 13, the intent is not to suggest causal relationships between disturbance speed and width upon amplitude. Ultimately, all these factors are influenced by a combination of initial conditions. Generally, it is found that experiments with small (large) lock-depth, D, relative to $\overline{H}$ produced an interfacial disturbance having small (large) amplitude, small (large) width, and slow (fast) speed. However, their values were additionally influenced by the relative stratification and ambient layer depths. A detailed investigation of these properties lies beyond the scope of the present study.

V. DISCUSSION AND CONCLUSIONS

Experimental results were presented that examined the behaviour of upslope propagating, partial-depth lock-release gravity currents in a two-layer ambient. The gravity currents were classified as supercritical, critical, or subcritical depending upon whether their observed speed was, respectively, faster than, approximately equal to, or slower than the observed speed of the interfacial disturbance generated by the forward advance of the gravity current. In most cases, the prediction for the initial gravity current front speed, developed from an extension of the prediction of Shin *et al.*,[11] was found to agree well with observations. When nondimensionalized by the characteristic speed based on the lock-fluid density and upper ambient density, the gravity current speed was found to be comparable to, but less than, the interfacial disturbance speed normalized by the two-layer long wave speed. Some of the supercritical gravity currents were found to decelerate and stop as predicted by (7) under the assumption that the deceleration is caused solely by the decreasing channel and lower-layer ambient depth. However, for almost all subcritical and for some critical gravity currents, the fronts stopped rapidly as a consequence of interactions with the interfacial disturbance. Similar observations have been made previously in related laboratory experiments.[22,23,30,33] The measured interfacial disturbance amplitude compared well with the semi-empirical prediction of Tan *et al.*,[19] albeit with a smaller value for the fitting parameter that relates the amplitude to the initial lock conditions. The half-width and speed of the interfacial disturbance were found to increase with amplitude. And, generally, the half-width, speed, and amplitude were larger in experiments having a greater initial height of dense gravity current fluid.

Qualitatively, we examined the evolution of the flows as the lower layer shallowed to zero depth. In the case of subcritical gravity currents that came to rest, the interfacial disturbance was observed to transform into a solitary wave that continued to propagate downstream at constant speed. The shoaling wave then transformed into a gravity current, all the while maintaining constant speed and amplitude. In cases of supercritical gravity currents, turbulence about the head was suppressed as the layer depth shallowed. After penetrating through the interface, the gravity current redeveloped turbulent structures as it propagated in the uniform density upper-layer ambient.

Future work will explore gravity currents propagating over non-uniform topography in uniform or stratified ambients to provide a model that more realistically captures coastal sea breezes interacting with atmospheric inversions.

ACKNOWLEDGMENTS

The authors would like to thank the reviewers for their helpful comments on the original manuscript. These experiments were inspired in part by conversations with Stuart Dalziel and the (unpublished) Ph.D. research of Matthew Brown performed in the mid-1990s at the University of Cambridge.

Some experiments were conducted by Dylan Podkowka (University of Alberta). This work was supported in part by funding from the Natural Sciences and Engineering Research Council through the Discovery Grant program.

[1] J. E. Simpson, "Gravity currents in the laboratory, atmosphere, and ocean," Annu. Rev. Fluid Mech. **14**, 213–234 (1982).
[2] J. E. Simpson, *Gravity Currents*, 2nd ed. (Cambridge University Press, Cambridge, England, 1997), p. 244.
[3] J. E. Simpson, *Sea Breeze and Local Winds* (Cambridge University Press, Cambridge, England, 1994), p. 234.
[4] G. H. Keulegan, "An experimental study of the motion of saline water from locks into fresh water channels," Technical Report No. 5168, National Bureau of Standards, 1957.
[5] G. H. Keulegan, "The motion of saline fronts in still water," Technical Report No. 5831, National Bureau of Standards, 1958.
[6] T. B. Benjamin, "Gravity currents and related phenomena," J. Fluid Mech. **31**, 209–248 (1968).
[7] J. E. Simpson, "Effects of lower boundary on the head of a gravity current," J. Fluid Mech. **53**, 759–768 (1972).
[8] H. E. Huppert and J. E. Simpson, "The slumping of gravity currents," J. Fluid Mech. **99**, 785–799 (1980).
[9] H. E. Huppert, "The propagation of two-dimensional and axisymmetric viscous gravity currents over a rigid horizontal surface," J. Fluid Mech. **121**, 43–58 (1982).
[10] J. W. Rottman and J. E. Simpson, "Gravity currents produced by instantaneous releases of a heavy fluid in a rectangular channel," J. Fluid Mech. **135**, 95–110 (1983).
[11] J. Shin, S. Dalziel, and P. Linden, "Gravity currents produced by lock exchange," J. Fluid Mech. **521**, 1–34 (2004).
[12] Z. Borden and E. Meiburg, "Circulation based models for Boussinesq gravity currents," Phys. Fluids **25**, 101301 (2013).
[13] G. F. Lane-Serff, L. M. Beal, and T. D. Hadfield, "Gravity current flow over obstacles," J. Fluid Mech. **292**, 39–53 (1995).
[14] P. G. Baines, "A unified description of two-layer flow over topography," J. Fluid Mech. **146**, 127–167 (1984).
[15] M. Ungarish, *An Introduction to Gravity Currents and Intrusions* (Chapman and Hall/CRC Press, New York, 2009), p. 489.
[16] J. Y. Holyer and H. E. Huppert, "Gravity currents entering a two-layer fluid," J. Fluid Mech. **100**, 739–767 (1980).
[17] M. R. Flynn, M. Ungarish, and A. W. Tan, "Gravity currents in a two-layer stratified ambient: The theory for the steady-state (front condition) and lock-released flows, and experimental confirmations," Phys. Fluids **24**, 026601 (2012).
[18] B. R. Sutherland, P. J. Kyba, and M. R. Flynn, "Interfacial gravity currents in two-layer fluids," J. Fluid Mech. **514**, 327–353 (2004).
[19] A. W. Tan, D. S. Nobes, B. A. Fleck, and M. R. Flynn, "Partial depth gravity currents in two-layer stratified media. Part 1: A study of the wave amplitude," in *International Conference on Environmental Science and Engineering* (World Academy of Science, Engineering and Technology, Singapore, 2010).
[20] C. Adduce, G. Sciortino, and S. Proietti, "Gravity currents produced by lock exchanges: Experiments and simulations with a two-layer shallow-water model with entrainment," J. Hydraul. Eng. **138**, 111–121 (2012).
[21] J. W. Rottman and J. E. Simpson, "The formation of internal bores in the atmosphere: A laboratory model," Q. J. R. Meteorol. Soc. **115**, 941–963 (1989).
[22] A. Mehta, B. R. Sutherland, and P. J. Kyba, "Interfacial gravity currents: Part II-wave excitation," Phys. Fluids **14**, 3558–3569 (2002).
[23] J. R. Munroe, C. Voegeli, B. R. Sutherland, V. Birman, and E. H. Meiburg, "Intrusive gravity currents from finite-length locks in a uniformly stratified fluid," J. Fluid Mech. **635**, 245–273 (2009).
[24] R. E. Britter and P. F. Linden, "The motion of the front of a gravity current travelling down an incline," J. Fluid Mech. **99**, 531–543 (1980).
[25] C. Cenedese and C. Adduce, "Mixing in a density driven current flowing down a slope in a rotating fluid," J. Fluid Mech. **604**, 369–388 (2008).
[26] A. Dai, "Experiments on gravity currents propagating on different bottom slopes," J. Fluid Mech. **731**, 117–141 (2013).
[27] A. Dai, "Non-Boussinesq gravity currents propagating on different bottom slopes," J. Fluid Mech. **741**, 658–680 (2014).
[28] L. J. Marleau, M. R. Flynn, and B. R. Sutherland, "Gravity currents propagating up a slope," Phys. Fluids **26**, 046605 (2014).
[29] V. Lombardi, C. Adduce, G. Sciortino, and M. L. Rocca, "Gravity currents flowing upslope: Laboratory experiments and shallow water simulations," Phys. Fluids **27**, 016602 (2015).
[30] T. Maxworthy, J. Leilich, J. Simpson, and E. H. Meiburg, "The propagation of a gravity current in a linearly stratified fluid," J. Fluid Mech. **453**, 371–394 (2002).
[31] K. G. Lamb, "Conjugate flows for a three-layer fluid," Phys. Fluids **12**, 2169–2185 (2000).
[32] B. L. White and K. R. Helfrich, "A general description of a gravity current front propagating in a two-layer stratified fluid," J. Fluid Mech. **711**, 545–575 (2012).
[33] A. W. Tan, D. S. Nobes, B. A. Fleck, and M. R. Flynn, "Gravity currents in two-layer stratified media," Environ. Fluid Mech. **11**, 203–224 (2010).
[34] J. Grue, A. Jensen, P.-O. Rusoàs, and J. K. Sveen, "Properties of large-amplitude internal waves," J. Fluid Mech. **380**, 257–278 (1999).
[35] B. R. Sutherland, K. J. Barrett, and G. N. Ivey, "Shoaling internal solitary waves," J. Geophys. Res. **118**, 1–14, doi:10.1002/jgrc.20291 (2013).